EPJ Web of Conferences **164**, 01017 (2017) DOI: 10.1051/epjconf/201716401017
ICNFP 2016

New results from T2K

A. Longhin[1,a] on behalf of the T2K Collaboration

[1] *Istituto Nazionale di Fisica Nucleare, Sez. di Padova, via Marzolo 8, 35131 Padova, Italy.*

Abstract. The T2K experiment is a 295-km long-baseline neutrino experiment in Japan employing an off-axis muon neutrino beam with a ~ 0.6 GeV peak energy. The beam, produced from 30-GeV protons at the J-PARC complex on the Pacific coast, is directed to the Super-Kamiokande detector. T2K released the first long-baseline measurement of a nonzero value for the θ_{13} mixing parameter through the observation of electron neutrino appearance ($\nu_\mu \rightarrow \nu_e$) and produced the most precise measurement of θ_{23} through the observation of muon neutrino disappearance ($\nu_\mu \rightarrow \nu_\mu$). T2K data, in combination with reactor experiments, also excludes at 90% C.L. a significant region of the Dirac CP phase: $\delta_{\rm CP} < -3.02(-1.87)$ and $\delta_{\rm CP} > -0.49(-0.98)$ for the normal (inverted) hierarchy. A full joint appearance and disappearance fit including both neutrino (7×10^{20} protons on target, PoT) and anti-neutrino (4×10^{20} PoT) data and, for the first time, a constraint from water target data in the near detector, is presented yielding improved sensitivity on $\delta_{\rm CP}$ and improved precision on $\sin^2 2\theta_{23}$ and the atmospheric mass splitting.

1 The T2K experiment

T2K is a long-baseline neutrino oscillation experiment located in Japan, exploiting 30 GeV protons from the Japan Proton Accelerator Research Center (J-PARC, in Tōkai, Ibaraki Prefecture) to create a muon neutrino beam. The proton beam is directed onto a graphite target and the resulting pions and kaons focussed by a system of three magnetic horns into a 96 m-long decay tunnel filled with helium gas. Depending on the direction of the 250 kA pulsed current, horns can select either positively charged particles, for a beam composed mainly of ν_μ (ν-mode), or negatively charged particles, for a beam composed mainly of $\bar{\nu}_\mu$ ($\bar{\nu}$-mode).

The neutrino beam is measured by two near detectors (INGRID, ND280) located 280 m from the target and a far detector, Super-Kamiokande (SK). The far detector and one of the near detectors (ND280) are placed 2.5° off-axis with respect to the protons' direction, which results in a narrow neutrino energy spectrum with a peak at about 0.6 GeV. The baseline between neutrino production and the far detector, 295 km, is chosen to correspond to the first minimum in the ν_μ survival probability at the peak energy.

T2K can measure neutrino oscillation in two channels: ν_μ disappearance ($\nu_\mu \rightarrow \nu_\mu$), which is dominated by the oscillation parameters $\sin^2 2\theta_{23}$ and Δm^2_{32} and ν_e appearance ($\nu_\mu \rightarrow \nu_e$), which is sensitive to $\sin^2 2\theta_{13}$, the octant of θ_{23} and through subleading terms to $\delta_{\rm CP}$ and the mass hierarchy[1]

[a] e-mail: longhin@pd.infn.it

[1] "Normal" mass hierarchy (NH) indicates the $\Delta m^2_{32}, \Delta m^2_{31} > 0$ case (state m_3 having the largest mass) while the other case is denoted as "inverted" mass hierarchy (IH).

via matter effects [2]. Variations in δ_{CP} induce asymmetries in the probabilities for the CP-conjugate channels $\nu_\mu \to \nu_e$ and $\bar{\nu}_\mu \to \bar{\nu}_e$. Negative values of $\sin\delta_{CP}$ enhance $\nu_\mu \to \nu_e$ and suppresses $\bar{\nu}_\mu \to \bar{\nu}_e$ oscillations and vice versa.

T2K has been taking data since 2010. The beam power has been steadily increasing (see Fig. 1) and stable running at 420 kW beam power was achieved in 2016. From mid-2013 until spring 2016, the beam ran in $\bar{\nu}$-mode. The event rates in $\bar{\nu}$-mode are significantly lower than in the ν-mode beam, mainly due to the lower $\bar{\nu}$ cross section and secondly to charge asymmetries in hadroproduction. Sensitivity studies show that the optimal strategy to constrain δ_{CP} is achieved when collecting roughly equal amounts of ν-mode and $\bar{\nu}$-mode protons on target (PoT) [1]. Using both beam polarities T2K can test the PMNS framework and search in an optimal way for CP violation ($\sin\delta_{CP} \neq 0$) implying $P(\nu_\mu \to \nu_e) \neq P(\bar{\nu}_\mu \to \bar{\nu}_e)$ or CPT violation or non-standard matter effects by comparing $P(\nu_\mu \to \nu_\mu) = P(\bar{\nu}_\mu \to \bar{\nu}_\mu)$. The results considered in this report are based on a sample of 1.1×10^{21} PoT, 0.7 and 0.4 $\times 10^{21}$ in ν-mode and $\bar{\nu}$-mode respectively (the full Run 1–7b data set).

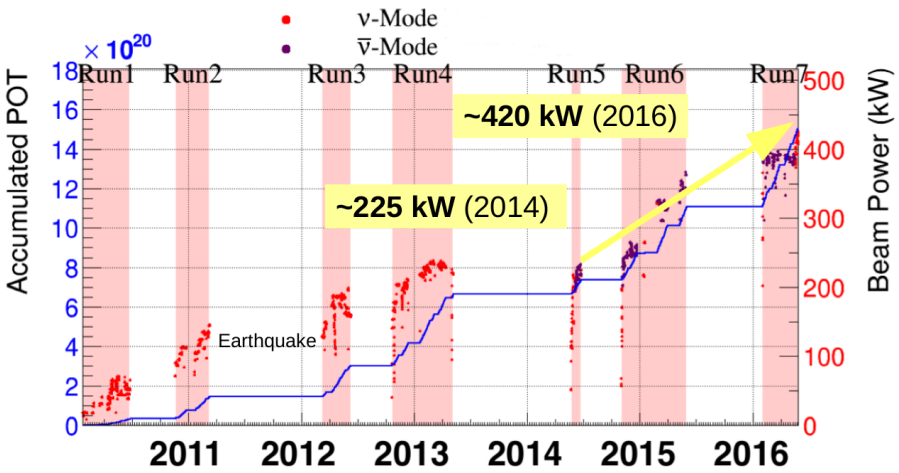

Figure 1. Time evolution of the integrated PoT (cumulative histogram, left side scale) and beam power on target (markers, right side scale).

1.1 The neutrino beam

A data-driven simulation is used to predict the neutrino flux from the T2K beam line. It is based on FLUKA (primary proton-target interactions) and the GEANT3 (propagation, reinteractions) Monte Carlo and incorporates data from the NA61/SHINE experiment [2–4], which has provided measurements of the hadron production cross sections using a thin carbon and a T2K replica target [5]. Beam monitor data (direction, profile and stability) as measured by the on-axis near detector INGRID [6], are also used as inputs to estimate the flux and its systematic uncertainty, currently at the $O(10\%)$ level [7]. The predicted fluxes in both ν and $\bar{\nu}$ modes at SK are shown in Fig. 2.

[2]Matter effects are moderate due to the 295 km baseline amounting at most to ~ 1/3 of the effects ruled by δ_{CP}.

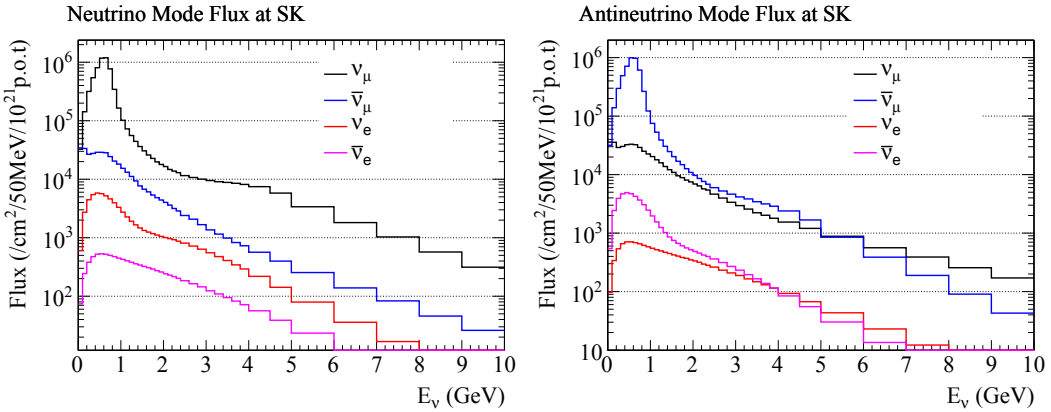

Figure 2. Predicted fluxes at the SK detector in the absence of oscillation effects for ν-mode (left) and $\bar{\nu}$-mode (right).

1.2 The near detectors: ND280 and INGRID

The INGRID [6] near detector (Fig. 3, left) is aligned with the proton beam axis while ND280 (Fig. 3, right) is at the same effective off-axis angle as SK. INGRID, is an array of iron/scintillator (scintillator/water) detectors arranged in a cross shape centered on the beam axis. The beam direction has been shown to be stable within 0.4 mrad.

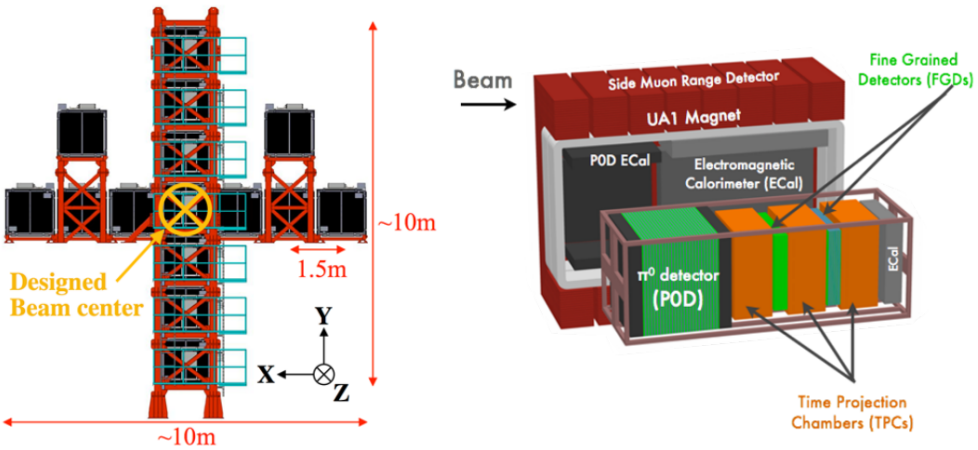

Figure 3. The T2K near detectors. Left: INGRID (on-axis). Right: ND280 (2.5°) off-axis.

ND280 consists of several sub-detectors installed inside the refurbished UA1/NOMAD magnet, providing a 0.2 T uniform magnetic field for charge identification. Three time projection chambers (TPC [8]) are interleaved with two fine-grained detectors (FGD [9]). The upstream FGD detector

(FGD1) is composed of 15 scintillators layers, while the downstream one (FGD2) contains 7+6 scintillator+water alternated layers. Energy loss in the TPC gas and track bending allow for good particle identification. ν_μ and $\bar{\nu}_\mu$ interactions are separated by tagging the primary $\mu^\pm$ and the neutrino energy can be measured (especially for charged-current quasi-elastic interactions, CCQE, where, to a good approximation, it only depends on lepton kinematics). ND280 data (in particular from TPCs and FGD 1, 2) are used directly in the oscillation fits to reduce the flux and cross-section uncertainties and provide a data-driven contraint to the expected number of interactions at SK.

1.3 The far detector: Super-Kamiokande

SK [10] is a 50 kt (22.5 kt fiducial) water Cherenkov detector located 1000 m underground in the Kamioka mine in the Japanese Alps (Gifu Prefecture). The water volume is divided into an outer detector which acts as a veto for entering particles (1885 outward-facing 8-inch photomultipliers - PMTs) and an inner detector lined with 11129, 20-inch PMTs for imaging Cherenkov rings. SK is capable of very good μ/e separation by the pattern of Cherenkov light cones from the charged lepton.

2 The oscillation analysis

The T2K oscillation results feature a joint appearance and disappearance fit using the ν-mode and $\bar{\nu}$-mode data. Data samples of charged current (CC) interactions are fit at ND280 to provide a tuned prediction of the unoscillated spectrum at the far detector and its associated uncertainty. This is then compared to the data at the far detector, where μ-like or e-like data samples are fit to estimate the oscillation parameters.

2.1 The near detector fit

The near detector fit takes inputs from the flux, cross section and detector models with associated uncertainties. The cross-section and flux uncertainties in the predicted rates at SK are reduced by fitting the parameter values in the underlying models. The differences in target materials in the near detector (carbon, oxygen) and far detector (primarily oxygen) is dealt by including large prior uncertainties as the differences in the interactions on different nuclei are not well understood. Separate parameters are used for Fermi momentum, binding energy, multinucleon event normalisation and CC coherent pion production nomalisation on oxygen. The flux model takes into account the correlations between the neutrino fluxes at the near and far detectors.

The ν-mode ν_μ-CC candidates originating in the FGD fiducial volumes are split into three samples depending on the number of tagged pions: CC0π, CC1π^+ and CC-other. In terms of interaction processes these samples are dominated by CCQE interactions ($\nu_\mu n \rightarrow \mu^- p$ or $\bar{\nu}_\mu p \rightarrow \mu^+ n$, the SK golden sample), CC resonant pion production and deep inelastic scattering, respectively [12]. For $\bar{\nu}$-mode data, both ν_μ and $\bar{\nu}_\mu$ CC interactions are selected and then divided into two subsamples, defined by the number of reconstructed tracks: $\bar{\nu}_\mu$ (ν_μ) CC-1-track, dominated by CCQE interactions and $\bar{\nu}_\mu$ (ν_μ) CC-N-tracks consisting of resonant production and deep inelastic scattering [13].

An important update in the near detector analysis is the use of interactions in the water modules of FGD2 which allow reducing the uncertainties related to the extrapolation across differing nuclear targets in the near and far detectors.

Using FGD1 and FGD2 interaction samples separately results in a total of six samples in ν-mode and eight samples in $\bar{\nu}$-mode. The binned distributions in p_μ and $\cos\theta_\mu$ for the 14 samples are fitted simultaneously to constrain parameters representing the systematic uncertainties in the flux and

	ν-mode		$\bar{\nu}$-mode	
Total	1-ring μ-like	1-ring e-like	1-ring μ-like	1-ring e-like
without constraint	12.0%	11.9%	12.5%	13.7%
with constraint	5.0%	5.4%	5.2%	6.2%

Table 1. Relative total systematic error on the number of expected neutrino interactions in SK (single-ring e-like and μ-like) before and after the near detector data constraint.

interaction models. As an example, the muon momentum distributions are shown in Fig. 4 for the CC-0π, CC-1π^+ and CC-other samples in ν-mode in FGD1 before (top row) and after (bottom row) the ND280 fit.

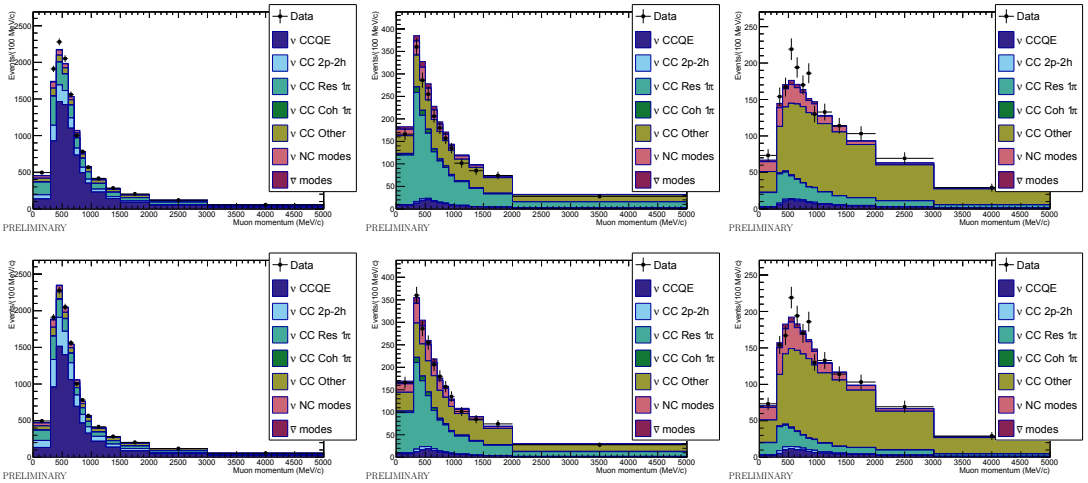

Figure 4. Example distributions of momentum for the muon candidate for the CC-0π (left column), CC1π (middle column) and CC other (right column) samples in the FDG1 fiducial volume. The upper row shows the distributions before the ND280 fit while the distributions after the fit are in the lower row (see Sect. 2.1).

The goodness of fit is 8.6%. The reduction of the uncertainty on the expected number of events at SK is substantial passing from 12–14% to 5–6%, as it can be seen in Tab. 1. The overall error is dominated by the cross-section parameters which are not constrained by the near detector (in particular the multinucleon event normalisation systematic).

2.2 Far detector fit

To enhance the purity of the selected sample in CCQE interactions candidates must have a single identified Cherenkov ring associated to the outgoing lepton. The neutrino energy (E_ν) for CC-QE interactions can be reconstructed from momentum and direction of the lepton assuming a two body interaction. Candidates must be on time with the accelerator, fully contained in the fiducial volume and must have $E_\nu < 1.25$ GeV.

The ν_μ and $\bar{\nu}_\mu$ samples are defined by a single ring muon-like pattern (1Rμ) with a visible energy (E_{vis}) above 200 MeV and having at most one delayed electron signature (from the primary μ decay).

The ν_e and $\bar{\nu}_e$ samples are defined by a single ring electron-like candidatee (1Re) with $E_{vis} > 100$ MeV and no decay electrons that may signal the presence of pions in the event. In addition the 1Re events are classified by a likelihood discriminator that separates out events containing a π^0. The number of events selected at each step in the ν_e selection chain are shown in the upper plots of Fig. 5 for ν and $\bar{\nu}$-modes both for data (bullets) and Monte Carlo (histogram). The distributions of the reconstructed neutrino energy for the final ν_e or $\bar{\nu}_e$ in both beam modes are shown in the bottom plots of the same figure.

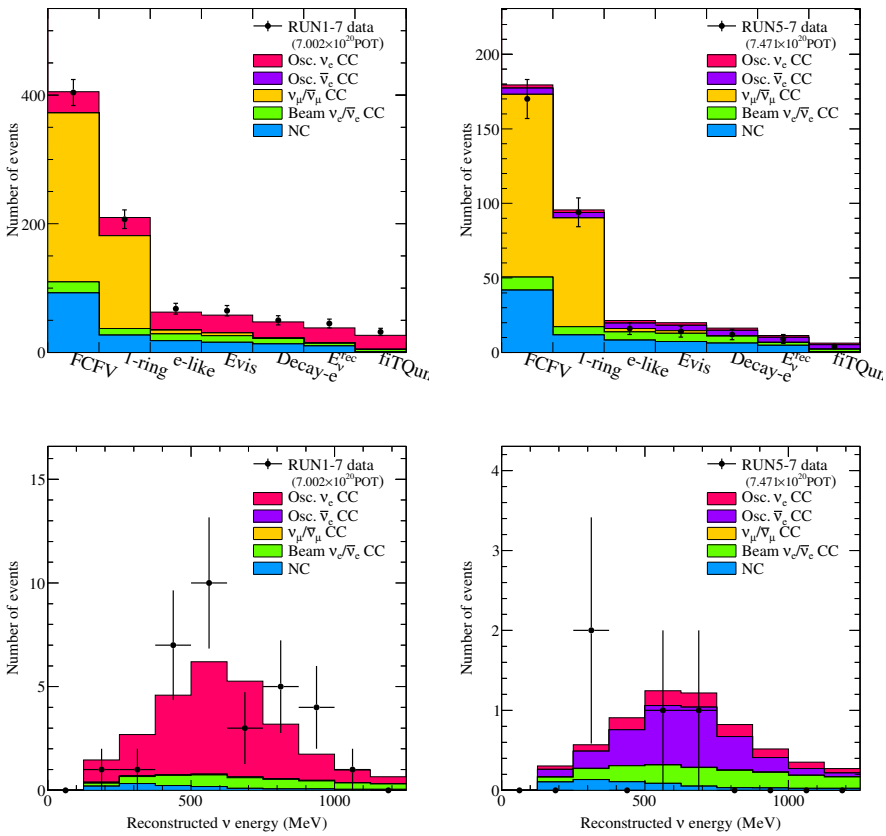

Figure 5. Reconstructed energy distributions for ν_e candidates in ν-mode running (left) and $\bar{\nu}_e$ candidates in $\bar{\nu}$-mode running (right). "Osc." stands for "Oscillated" and indicates the ν_e component arising from $\nu_\mu \rightarrow \nu_e$ transitions. The most relevant backgrounds are the intrinsic ν_e or $\bar{\nu}_e$ components in the beam and Neutral Current (NC) interactions due to π^0 production.

T2K observes a total of 32 ν_e candidate events in the far detector with a purity above 80% and 4 $\bar{\nu}_e$ candidates with $\sim 50\%$ purity. The reconstructed energy distributions of the 125 ν_μ candidates in ν-mode running are shown in the left plot of Fig. 6. The same distribution for the 66 $\bar{\nu}_\mu$ candidates in $\bar{\nu}$-mode running is shown by the right-side plot in the same figure.

Table 7 shows the measured and expected event rates under different assumptions for the $\delta_{\rm CP}$ phase: 0, $\pm\pi/2$, π. In ν-mode, the observed 1Re events are larger than the expected ν_e appearance

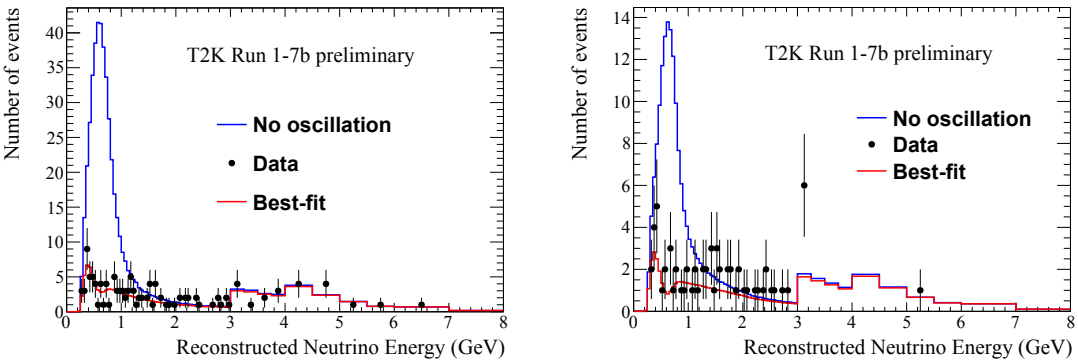

Figure 6. Reconstructed energy distributions for ν_μ candidates in ν-mode running (left) and $\bar{\nu}_\mu$ candidates in $\bar{\nu}$-mode running (right). Left: best-fit neutrino reconstructed energy spectra for the ν-mode μ-like sample corresponding to the Run 1–7b statistic (red). The distribution is obtained by fitting $\sin^2\theta_{23}$, $\delta_{\rm CP}$ and mass hierarchy with reactor constraint and marginalising all the systematic parameters. The best-fit distributions are compared with the predicted unoscillated spectrum (blue) as well as the Run 1–7b data set (black dots). Right: anti-ν mode.

Normal hierarchy						
Beam mode	Sample	$\delta_{CP}=-\pi/2$	$\delta_{CP}=0$	$\delta_{CP}=+\pi/2$	$\delta_{CP}=\pi$	Observed
neutrino	μ-like	127.5	127.2	127.4	127.7	125
neutrino	e-like	26.9	22.7	18.4	22.7	32
antineutrino	μ-like	64.2	64.1	64.2	64.4	66
antineutrino	e-like	6.0	6.9	7.7	6.8	4
Inverted hierarchy						
Beam mode	Sample	$\delta_{CP}=-\pi/2$	$\delta_{CP}=0$	$\delta_{CP}=+\pi/2$	$\delta_{CP}=\pi$	Observed
neutrino	μ-like	126.9	127.1	126.8	126.6	125
neutrino	e-like	23.9	20.0	16.1	20.0	32
antineutrino	μ-like	63.8	64.0	63.8	63.7	66
antineutrino	e-like	6.5	7.4	8.4	7.4	4

Figure 7. Expected event rate for SK sample for each mass hierarchy and the following values of $\delta_{\rm CP}$. $-\pi/2$, 0, $+\pi/2$, π. The other oscillation parameters are fixed to $\sin^2\theta_{13}=0.0217$, $\sin^2\theta_{23}=0.528$, $\Delta m^2_{32}(\Delta m^2_{13})=2.509\times10^{-3}eV^2/c^4$, $\sin^2\theta_{12}=0.846$, $\Delta m^2_{21}=7.53\times10^{-5}eV^2/c^4$. The observed event rate during the Run 1–7b data taking is also shown.

events for any choice of $\delta_{\rm CP}$, the lowest difference happening for $\delta_{\rm CP}=-\pi/2$ while in $\bar{\nu}$-mode the observation lies below the expectation also in this case favoring $\delta_{\rm CP}=-\pi/2$ which is the value inducing the largest ν-$\bar{\nu}$ asymmetry. This behavior in the observed data is such that the resulting constraints on $\delta_{\rm CP}$ are tighter than what is expected given the sensitivity of the measurement (see Fig. 9).

The result of the near detector fit is propagated to the far detector. This is used as a prior for the far detector fit, which includes additional uncertainties from the SK detector model. The electron and muon samples in the ν-mode and $\bar{\nu}$-mode are fitted simultaneously with nuisance parameters shared between the samples. The results in the $\delta_{\rm CP}$-$\sin^2 2\theta_{13}$ space are shown in Fig. 8. The θ_{13} determination

is consistent with the reactor measurement and data show a preference for the maximally CP-violating value of $\delta_{\rm CP} = -\pi/2$ which enhances $\nu_\mu \to \nu_e$ and suppresses $\bar{\nu}_\mu \to \bar{\nu}_e$.

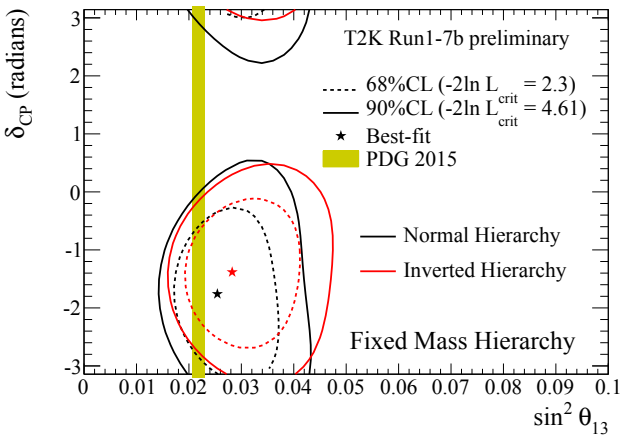

Figure 8. Measured $\Delta\chi^2$ distributions as a function of $\sin^2\theta_{13}$, $\delta_{\rm CP}$ and mass hierarchy with the full Run 1–7b data set. Both normal (black solid line) and inverted (black dashed line) hierarchies are shown. The constant $\Delta\chi^2$ critical values in the gaussian approximation are shown. The mass hierarchy was fixed, i.e. the contours are not produced with common χ^2 minimum value. All the oscillation parameters which are not parameters of interest are marginalised. The reactor constraint is not applied.

Figure 9 (left) shows the observed $\Delta\chi^2$ as a function of $\delta_{\rm CP}$ and mass hierarchy (black is NH, red IH), with the reactor constraint on $\sin^2 2\theta_{13}$ [14–16]. The 90% confidence levels are built with the Feldman-Cousins method, resulting in intervals of [-3.02, -0.49] for NH and [-1.87, -0.98] for IH. CP conservation ($\sin\delta_{\rm CP} = 0$) is excluded then for both mass hierarchy hypotheses at 90% confidence level. Toy Monte Carlo studies indicate that if $\delta_{\rm CP} = -\pi/2$ the probability to exclude $\delta_{\rm CP} = 0$ or $\pm\pi$ with present data is about 20%. The right plot in Fig.9 shows the expected contraints achievable on average on $\delta_{\rm CP}$ with this data sample. In these plots both NH and IH $\Delta\chi^2$ are with reference to the same global minimum which occurs in the NH hypothesis. All the oscillation parameters which are not parameters of interest are marginalised. The global values from PDG 2016 are used as uncertainties on $\sin^2\theta_{13}$, $\sin^2\theta_{12}$ and Δm^2_{21}.

The ν_μ and $\bar{\nu}_\mu$ selection shown in Fig. 6 and Tab. 7 show maximal disappearance occurring exactly in the highest statistics region of the energy spectrum of interacting neutrinos providing world-leading constraints in the $\sin^2\theta_{23}$ and Δm^2_{23} parameters as shown in left plot of Fig. 10. The T2K contour (black) is obtained using $\Delta\chi^2$ critical values in the gaussian approximation. All the oscillation parameters which are not parameters of interest are marginalised. The reactor constraint on θ_{13} is applied. The T2K contour is compared to the other experiment results (SK [18], MINOS+, NOνA [19] and IceCube DeepCore [20]). In the right plot of Fig. 10 it can be seen how T2K data tend to favour maximal disappearance ($\sin^2 2\theta_{23} = 1$) also when fitting ν_μ (red) and $\bar{\nu}_\mu$ (blue) data separately. The best fit for NH occurs at $\sin^2 2\theta_{23} = 0.532^{+0.044}_{-0.060}$ and $\Delta m^2_{23} = 2.545^{+0.084}_{-0.082}$ while at $\sin^2 2\theta_{23} = 0.534^{+0.041}_{-0.059}$ and $\Delta m^2_{23} = 2.510^{+0.082}_{-0.083}$ for IH.

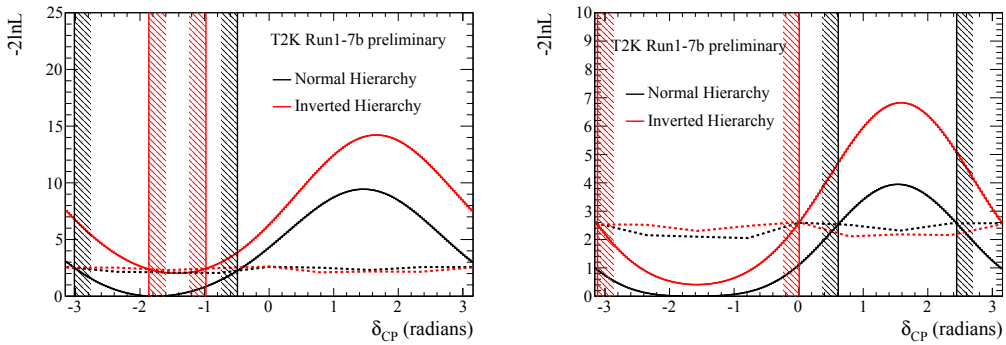

Mass Hierarchy	Allowed region at 90% CL (radians)
Normal	$-3.02 \leq \delta_{CP} \leq -0.49$
Inverted	$-1.87 \leq \delta_{CP} \leq -0.98$

Figure 9. Observed (left) and expected (right) 90% CL intervals on $\delta_{\rm CP}$. Left: measured allowed 90% CL intervals for $\Delta\chi^2$ distributions as a function of $\delta_{\rm CP}$ and mass hierarchy with the Run 1–7b data set. Both normal (black lines) and inverted (red lines) hierarchies are shown. Right: expected allowed 90% CL intervals assuming ($\delta_{\rm CP} = -1.601$, $\theta_{23} = 0.528$ and $\Delta m^2_{32} = 2.509 \times 10^{-3} eV^2/c^4$ (Δm^2_{13}).

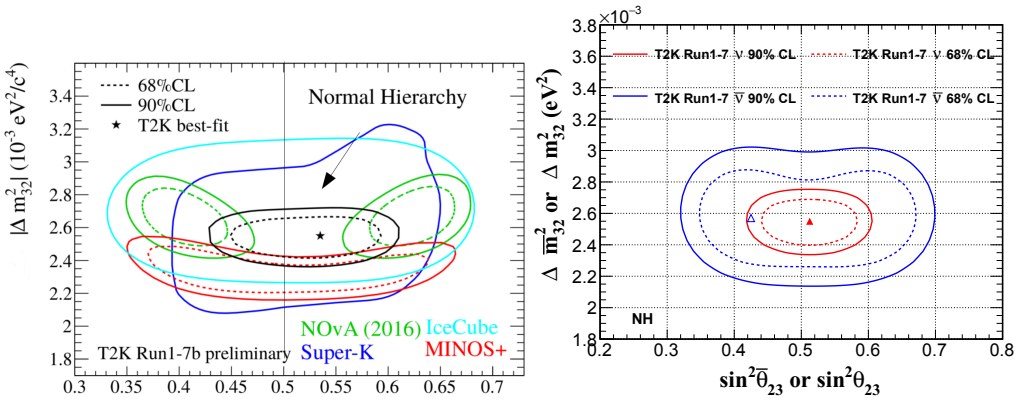

Figure 10. Left: Measured $\Delta\chi^2$ distributions as a function of $\sin^2\theta_{23}$, $\Delta m^2_{32}(\Delta m^2_{13})$ and mass hierarchy with the full Run 1–7b data set. The mass hierarchy is fixed to normal. Right: comparison of T2K ν_μ (red) and $\bar{\nu}_\mu$ (blue) data.

3 Summary and future prospects

The results of a joint analysis of ν and $\bar{\nu}$ oscillations at T2K with the ν_μ ($\bar{\nu}_\mu$) disappearance and $\nu_\mu(\bar{\nu}_\mu) \rightarrow \nu_e(\bar{\nu}_e)$ appearance channels, based on 7×10^{20} PoT in ν-mode and 4.0×10^{20} in $\bar{\nu}$-mode have been presented. Data show a preference for maximal θ_{23} mixing with no hints for a violation of the CPT theorem. In the appearance channel, we observe a tendency for large ν_e appearance and a low $\bar{\nu}_e$ appearance with respect to expectations. This favours the $\delta_{\rm CP} \sim -\pi/2$ solution, with a 90% confidence

interval of $[-3.02, -0.49]$ in normal mass hierarchy hypothesis and $[-1.87, -0.98]$ in inverted mass hierarchy. The first combined neutrino and anti-neutrino oscillation analysis at T2K is well-advanced.

3.1 The T2K-II phase

T2K was originally approved to collect 7.8×10^{21} PoT by 2021. An extension of the experiment (T2K-II phase) has been proposed recently aiming at a three-fold increase in the baseline sample by 2026 (20×10^{21} PoT). This goal can be met by a staged upgrade program of the accelerator beamlines. The first-stage of the program has been approved to improve the J-PARC Main Ring power supplies and reduce the machine cycle from 2.48 s to 1.3 s, allowing the beam power to be raised from the current 420 kW to ~ 800 kW. Further accelerator and secondary beamline upgrades will allow it to reach 1.3 MW. Figure 11 shows the expected future trends in terms of accelerator power and collected PoT. Further improvements will allow the magnetic horns to be operated with an increased current

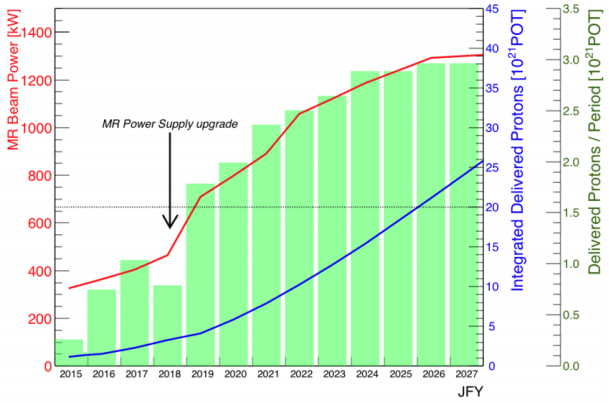

Figure 11. Projection of PoT (blue curve) and power on target (red curve) for the T2K-II program.

from 250 to 320 kA, an optimization of the far detector fiducial volume and of the samples used in the analysis. This could allow a 50% increase in the effective PoT.

The potential impact of the outlined program is quite significant: it may allow T2K-II to exclude CP conservation at more than 3 σ for any value of θ_{23} provided that the true value would turn out to be the currently favoured one i.e. $\delta_{CP} = -\pi/2$ (see Fig. 12).

References

[1] K. Abe et al. (T2K Coll.) PTEP 2015 (2015) no.4, 043C01
[2] N. Abgrall et al. (NA61/SHINE Coll.), Phys. Rev. C 85, 035210 (2012).
[3] N. Abgrall et al. (NA61/SHINE Coll.), Phys. Rev. C 84, 034604 (2011).
[4] N. Abgrall et al. (NA61/SHINE Coll.), Eur. Phys. J. C76, 84 (2016).
[5] N. Abgrall et al. (NA61/SHINE Coll.), Eur. Phys. J. C76 11, 617 (2016).
[6] K. Abe et al. (T2K Coll.), Nucl. Instrum. Methods A694, 211 (2012).
[7] K. Abe et al. (T2K Coll.), Phys.Rev. D87 (2013) no.1, 012001
[8] N. Abgrall et al. (T2K ND280 TPC Coll.), Nucl. Instrum. Methods A637, 25 (2011).

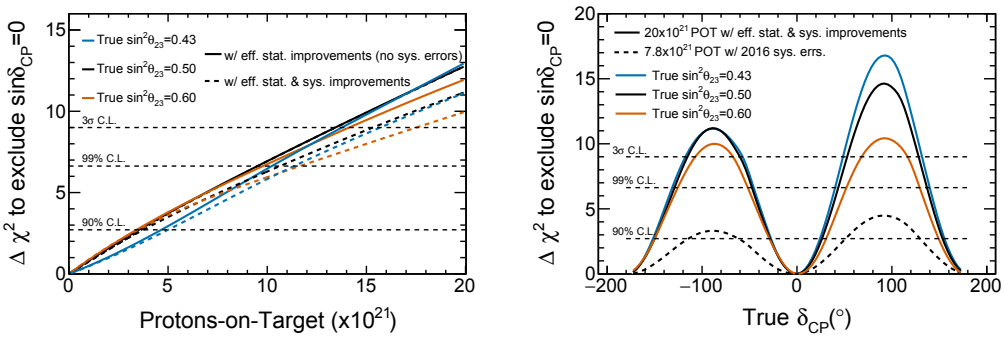

Figure 12. T2K-II physics reach. $\Delta\chi^2$ to exclude $\sin\delta_{\mathrm{CP}} = 0$ as a function of PoT with a 50% effectively statistic improvement of T2K Phase 2 statistics and improved systematic errors. The $\delta_{\mathrm{CP}} = -\frac{\pi}{2}$ and normal mass hierarchy are assumed to be true. Right: $\Delta\chi^2$ to exclude $\sin\delta_{\mathrm{CP}} = 0$ as function of true δ_{CP}. Sensitivities at different values of $\sin^2\theta_{23}$ (0.43, 0.5, 0.63) are compared. Mass hierarchy is assumed to be known.

[9] P. Amaudruz et al. (T2K ND280 FGD Coll.), Nucl. Instrum. Methods A696, 1 (2012).
[10] K. Abe et al. Nucl. Instrum. Meth., A659, 106-135, 2011.
[11] K. Abe et al. (T2K Coll.), Nucl. Instrum. Methods A659, 106 (2011).
[12] K. Abe et al. (T2K Coll.), Phys. Rev. D91, 072010 (2015).
[13] K. Abe et al. (T2K Coll.), Phys. Rev. Lett. 116 (2016) no.18, 181801.
[14] F. P. An et al. Phys. Rev. Lett., 108, 171803, 2012.
[15] J. K. Ahn et al. Phys. Rev. Lett., 108, 191802, 2012.
[16] Y. Abe et al. Phys. Rev. Lett., 108, 131801, 2012.
[17] K. Abe et al. e-Print: 1609.04111.
[18] R. Wendell PoS ICRC2015 (2015) 1062.
[19] P. Adamson et al. (NOνA Coll.), Phys. Rev. D93 (2016) 051104, e-Print: 1601.05037.
[20] M. G. Aartsen et al. (IceCube Coll.), Phys.Rev. D91 (2015) 072004, e-Print: 1410.7227.